



1 Rapidly Changing Lake-Terminating Glaciers in High

2 Mountain Asia: A Dataset from 1990 to 2022

- 3 Yunyi Luo^{1,2}, Qiao Liu¹, Xueyuan Lu^{1,2}, Yongsheng Yin^{1,2}, Jiawei Yang^{1,2}, Xuyang
- 4 Lu
- 5 1 Institute of Mountain Hazards and Environment, Chinese Academy of Sciences, Chengdu 610041,
- 6 China
- 7 2 College of Resources and Environment, University of Chinese Academy of Sciences, Beijing 100049,
- 8 China
- 9 Correspondence: Qiao Liu; liuqiao@imde.ac.cn
- 10 Abstract. Lake-terminating glaciers (LTGs) typically exhibit higher rates of retreat and thinning 11 compared to land-terminating glaciers. However, a comprehensive inventory for LTGs and their 12 associate proglacial lakes across High Mountain Asia (HMA) is currently lacking, limiting further 13 understanding of their spatial heterogeneity in glacier change. This study employs a semi-automated 14 identification method, coupled with rigorous visual inspection, to construct a comprehensive inventory 15 of LTGs and proglacial lakes in HMA for 1990 and 2022. Our data indicate that, by 2022, HMA hosted 16 $1740 \text{ LTGs} (5082.08 \pm 13.15 \text{ km}^2)$, among which $667 \text{ glaciers} (3454.59 \pm 12.43 \text{ km}^2)$ remained in contact 17 with proglacial lakes since 1990, 1073 (1627.49 \pm 4.30 km²) are newly developed and 468 (960.13 \pm 18 3.18 km²) had disconnected from proglacial lakes during the investigation period. Accordingly, 645 19 proglacial lakes (207.18 \pm 0.82 km²) remained in contact with ice, 1123 new lakes (54.85 \pm 0.35 km²) 20 formed, and 485 lakes (45.31 ± 0.34 km²) detached from ice (including 25 disappeared). During the past 21 32 year, the total area of proglacial lakes increased by 138.19 ± 1.18 km² (81.7%), alongside a glacier 22 area loss of $324.43 \pm 19.23 \text{ km}^2$ (5.1%). The southern regions of HMA, particularly the Hindu Kush, 23 Himalayas, Nyainqentanglha, and Gangdise Mountains, exhibiting the highest concentration and rapidest 24 changes of the glacier-lake system. We hope that this dataset will improve our understanding of mountain 25 glacier-lake interactions, water availability, as well as glacier-related hazards in HMA. 26 The dataset is available at https://doi.org/10.5281/zenodo.17369580 (Luo and Liu, 2025).





1 Introduction

27

28

29

30

31

32

33

34

35

36

37

38

39

40

41

42

43

44

45

46

47

48

49

50

51

52

53

54

al., 2020; Truffer and Motyka, 2016; Chernos et al., 2016) and are a primary driver of spatial heterogeneity in glacier responses to climate change (Brun et al., 2019; Maurer et al., 2019). Proglacial lakes typically form behind end or lateral moraines, on debris-covered glaciers often developed through the coalescence of multiple supraglacial ponds near the glacier terminus (Carrivick and Tweed, 2013; Quincey et al., 2007; Mertes et al., 2017). The influence of lake water on glacier change operates primarily through two mechanisms: (1) thermal undercutting by lake water (Truffer and Motyka, 2016) and calving at the glacier front (Benn et al., 2007a), which together accelerate subaquatic and frontal ablation; and (2) when glacier termini come into contact with sufficiently deep water, the buoyancy of the lake reduces basal effective pressure, thereby enhancing glacier flow and dynamic thinning (Sugiyama et al., 2011; Sutherland et al., 2020; Benn et al., 2007b). (Sato et al., 2022; Tsutaki et al., 2019; Tsutaki et al., 2017). Observations indicate that LTGs in HMA have mass loss rates 18-97% higher than the regional average (Brun et al., 2019), and under comparable geographic conditions, their flow velocities are typically two- to threefold greater than those land-terminating counterparts. Furthermore, Zhang et al. (2023) reported that existing geodetic methods, by failing to account for the replacement of glacier ice by lake water, underestimate the mass loss of Himalayan LTGs by approximately 6.5%. HMA encompassing the entire Tibetan Plateau and its surroundings contains the largest concentration of mid-latitude mountain glaciers on Earth. Driven by ongoing global warming, glaciers in HMA have undergone a persistent negative mass balance, with an average mass loss rate of -20.1 Gt a-1 during 2000-2019 (Hugonnet et al., 2021). Glacier meltwater has driven substantial runoff and facilitated the formation and expansion of glacial lakes. From 1990 to 2018, the number of glacial lakes in HMA increased by 11%, and their total area expanded by 15% (Wang et al., 2020). The ongoing increase in both the number and extent of proglacial lakes underscores the critical need for a comprehensive assessment of lake-terminating glacier-proglacial lake systems in HMA. Such an evaluation is essential for elucidating feedback between the lake and ice, forecasting their responses to future climate change, and informing evidence-based strategies for water resource management and disaster risk mitigation. Although several regional-scale glacial lake inventories have been published in

Proglacial lakes in direct contact with glacier termini play a critical role in glacier evolution (Liu et



recent years (Wang et al., 2020; Chen et al., 2021; Zhang et al., 2015; Worni et al., 2013; Salerno et al., 2012; Shugar et al., 2020), most datasets do not distinguish the contact status and its change between glaciers and proglacial lakes. Moreover, there is currently no comprehensive inventory of lake-terminating glacier-proglacial lake systems covering the entire HMA, and their spatiotemporal evolution remains poorly understood. Therefore, this study aims to construct a dataset of LTGs and proglacial lakes for HMA based on multi-source remote sensing data, thereby filling this research gap and providing fundamental database to support studies on regional glacier change, water resource assessment, disaster management, and glacier hydrology.

2 Study area

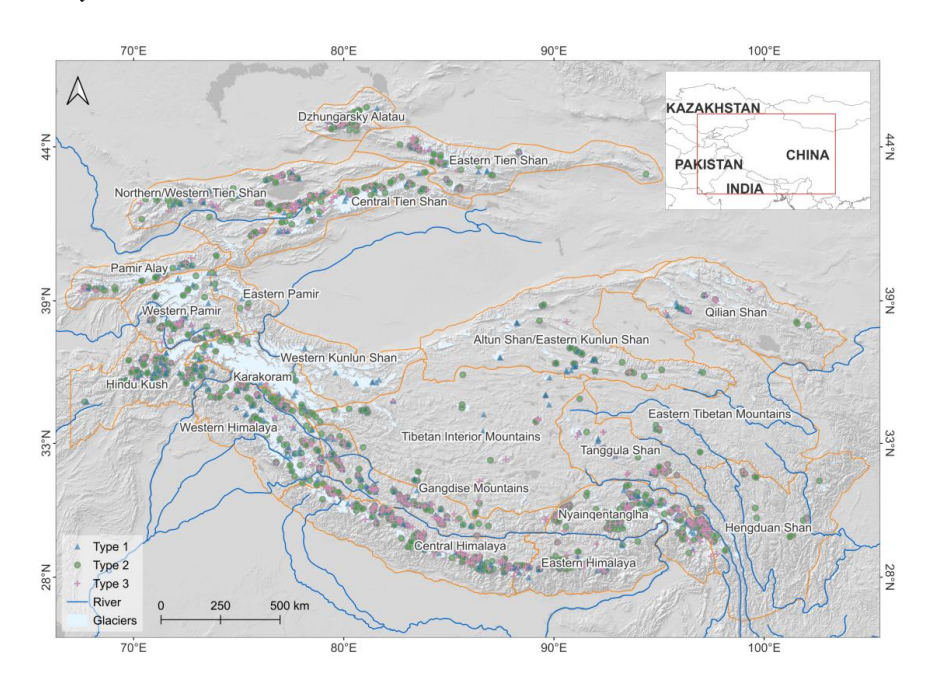


Figure 1: Location of HMA and distribution of LTGs. Glacier outlines from the Randolph Glacier Inventory (RGI v7.0). Types of LTGs are shown in Table 1.

High Mountain Asia (HMA), encompassing the Tibetan Plateau and its surrounding ranges-including the Himalayas, Karakoram, and Pamir Plateau, etc.-constitutes the most glacier-rich region in the mid-latitudes (Figure 1). HMA lies between 26°-45°N and 67°-105°E. It has an average elevation of approximately 4,500 m. The region features a complex topography. This topography is characterized by



higher elevations in the northwest and lower elevations in the southeast. It comprises a network of interwoven mountain ranges, valleys, and river systems. The dominant orographic orientation is east-west. The Tanggula Shan, located in the central part of the region, rise above 6,000 m, while the Himalayas contain 15 peaks exceeding 8000 m, and most peaks on the northern plateau surpass 6500 m. North-south trending ranges are mainly distributed in the southeastern Tibetan Plateau and the Hengduan Shan, forming the geomorphological framework of the region and controlling the overall topographic configuration of the plateau.

Climatically, the southern part of HMA is dominated by the South Asian and East Asian monsoons, bringing abundant precipitation, whereas the northern and western sectors are under the influence of the mid-latitude westerlies, characterized by arid conditions and scarce precipitation (Yao et al., 2012). This pronounced north-south climatic contrast results in a highly heterogeneous spatial pattern of glacier accumulation and ablation across the region. HMA serves as the source region for several major Asian rivers, including the Yellow River, Yangtze River, Yarlung Tsangpo, Indus, Ganges, Salween, Mekong, and Irrawaddy, which are vital for downstream hydrological processes and water resource availability. According to the Randolph Glacier Inventory (RGI 7.0), HMA hosts 94,058 modern glaciers, covering approximately 99,468.4km², making it the most extensively glacierized region outside polar areas. Most glaciers in HMA are undergoing retreat (Brun et al., 2017; Hugonnet et al., 2021). However, slight mass gains have been observed in parts of the Karakoram and western Kunlun ranges (Gardelle et al., 2012; Kääb et al., 2015), though recent studies suggest this trend may be diminishing (Hugonnet et al., 2021).

3 Data and methodology

3.1 Extraction of proglacial lake outlines

Before developing a comprehensive inventory of LTGs shown in Figure 1, we first generated a proglacial lake dataset using an automated delineation workflow within the Google Earth Engine (GEE) platform. We used Landsat imagery from the Thematic Mapper (TM) and Operational Land Imager (OLI) sensors, selected for their long-term record (since 1972), 30 m resolution, global coverage, and open access. All images were pre-processed in GEE, including radiometric, atmospheric, and geometric corrections. To minimize seasonal variability and the presence of snow and ice, we selected images



acquired from July to November. Two-time windows were defined: 1990 ± 2 years (historical) and
2022 ± 1 year (recent). Due to limited image availability around 1990, imagery from 1993 to 1996 was
used to supplement data gaps. A 2 km buffer around each glacier was applied to focus on potential ice-
contact proglacial lakes. Cloud contamination was reduced using the CFMask algorithm (Foga et al.,
2017) to detect and mask clouds and shadows, followed by compositing cloud-free mosaics (Figure 2ab).
In total, 4570 Landsat TM scenes were used for the 1990 period and 5493 OLI scenes for the 2020 period
(Figure 2cd).
Glacial lake extents were delineated using an automated mapping algorithm based on hierarchical
image segmentation and terrain analysis (Li and Sheng, 2012; Zhang et al., 2017). To reduce the influence
of mountain shadows, pixels with slopes $>20^\circ$ or shaded relief values <0.25 were excluded (Zheng et al.,
$2021). \ Previous \ studies \ applied \ varying \ minimum \ area \ thresholds \ for \ glacial \ lake \ identification: \ 0.0054$
$km^{2}\ (Wang\ et\ al.,\ 2020),\ 0.0081\ km^{2}\ (Chen\ et\ al.,\ 2021),\ 0.0036\ km^{2}\ (Luo\ et\ al.,\ 2020),\ and\ 0.01\ km^{2}\ (Lio\ et\ al.,\ 202$
et al., 2020). Smaller thresholds can lead to greater uncertainties due to the limitations of pixel resolution
(Salerno et al., 2012). To improve the accuracy of lake-terminating glacier identification, we adopted a
minimum lake area threshold of 0.0036 km² (equivalent to at least four pixels), following Luo et al.
(2020).

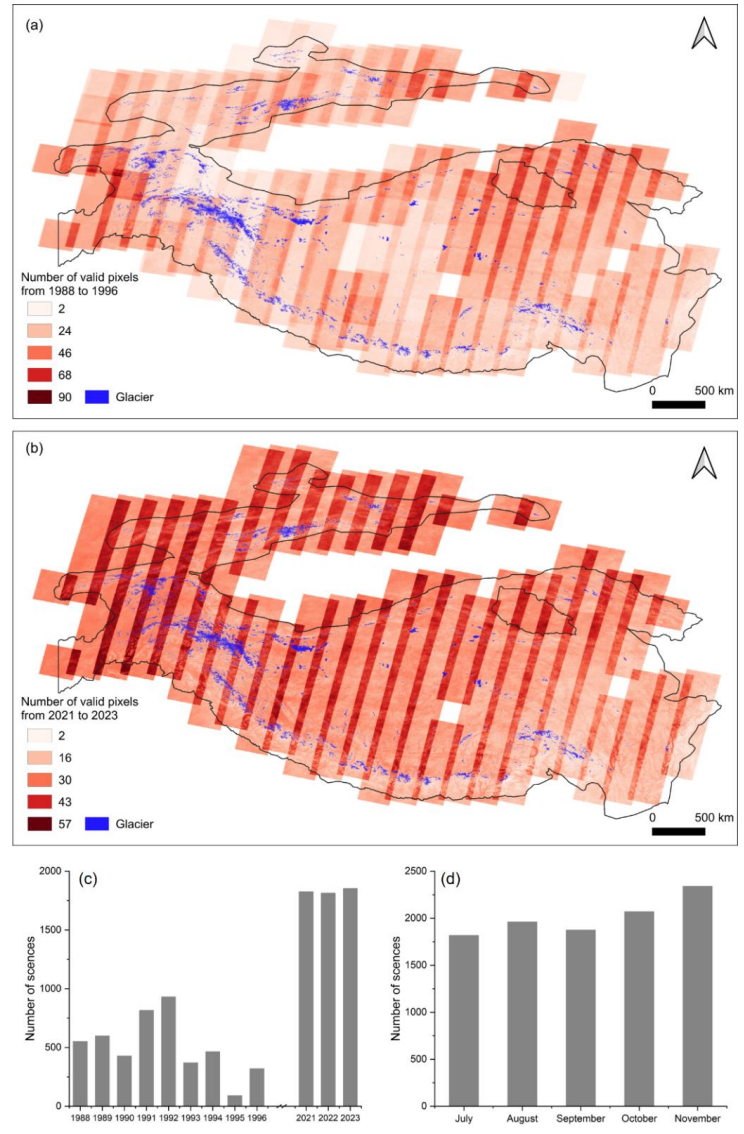


Figure 2: The number of usable pixels remaining in the study area after cloud removal during 1988–1996 (a) and 2021–2023 (b). Temporal distribution of the number of images used, by year (c) and by month (d).

3.2 Mapping of LTGs

114 115

116

117

118

119

120

121

In this study, LTGs are defined as glaciers that develop proglacial lakes along the direction of ice flow and are in direct contact with these lakes. The proglacial lake dataset was cross-referenced with the RGI 7.0 glacier inventory to identify LTGs. Results were refined through detailed visual inspection and manual correction using multi-source data, including Landsat and Planet Labs imagery, online maps (e.g.,

https://doi.org/10.5194/essd-2025-596 Preprint. Discussion started: 20 October 2025 © Author(s) 2025. CC BY 4.0 License.

122

123

124

125

126127

128

129

130

131

132

133

134

135

136

137

138





Google Earth, Esri basemap), and existing glacial lake datasets (Wang et al. 2020, Chen et al. 2021, Zhang et al. 2023). The identification of glacier-lake contact followed a two-step procedure. (1) Preliminary screening: A 500 m buffer was applied to assess spatial intersections between glacier boundaries and proglacial lakes, identifying potentially connected glacier-lake pairs. (2) Manual verification: Different criteria were applied for different periods. For the year 2020, multi-source moderate-to-high resolution imagery (e.g., Planet Labs, Landsat, Google Earth, Esri basemaps) was used. Glacier-lake contact was confirmed when proglacial lakes overlapped with glacier terminus and exhibited diagnostic geomorphic features, such as terminal ice cliffs or transverse crevasses perpendicular to the flow direction. Due to limited data availability and the relatively coarse spatial resolution of Landsat imagery (30 m) in 1990, direct identification of LTGs for that year involved considerable uncertainty, particularly for small glaciers, where boundary errors increase with decreasing glacier area. To address this, a temporal cross-validation approach was employed. Glaciers with ambiguous contact in 1990 were classified as interacting if satellite imagery from 1990 to 2022 showed lake expansion toward the glacier terminus. Based on the temporal evolution of glacier-lake contact, LTGs were categorized into three types (Table 1): (1) terminus persistent contacting with proglacial lake (Type 1); (2) terminus experencing transition from supraglacial lake to proglacial lake (Type 2); and (3) terminus detaching from proglacial lake (Type 3).



Table 1 The classification system of glaciers is based on the dynamic changes in glacier-lake contact. The basemap is derived from Landsat imagery.

Types	Characteristics			
Type 1	Persistent contact between glacier and lake from 1990 to 2022. Case location: 94,51053E, 30,63100N	0 2 km	0 200	16-Antown
Type 2	Transition from supraglacial lake to proglacial lake from 1990 to 2022. Case location: 88.23816E, 27.81772N	11. day. 920)	0 1 m	0 5 mm
Type 3	Detachment of the proglacial lake from the parent glacier from 1990 to 2022. Case location: 85.84583E, 28.20793N	(R)200 A	POCHED THE	640999

3.3 Uncertainty estimates

141

142

143

144

145

146

147

148

149

When interpreting glacial lake and glacier boundaries using remote sensing data, errors are inevitable even when manual visual delineation is applied. These errors are typically associated with various factors related to image quality, such as spatial resolution, cloud cover, mountain shadows, and subjective interpretation biases. Previous studies have reported that the area error in delineating glacier or glacial lake boundaries from remote sensing imagery is approximately ± 0.5 pixels, depending on the quality of the imagery. The uncertainty (δ) and relative error (E_l) of glacial lake area was estimated using the equation (Hanshaw and Bookhagen, 2014):

$$\delta = \frac{P}{G} \times \frac{G^2}{2} \times 0.6872 \tag{3}$$

$$E_l = \frac{\delta}{A} \times 100\% \tag{4}$$

where P is the perimeter of the glacial lake, and A is the glacial lake area.

The uncertainty (λ) and relative error (E_g) in glacier area was estimated to using the equation (Bolch et al., 2010):

$$\lambda = N \times \frac{G^2}{2} \tag{1}$$





 $E_g = \frac{\lambda}{S} \times 100\% \tag{2}$

where N is the total count of pixels along the outline of ice coverage, G is the spatial resolution of the images used, and S is the glacier area.

3.4 Attributes of inventory data

In this inventory, 9 attribute fields (Table 2) were recorded for the LTG, including a unique identifier, type, associated mountain range, area, mapping uncertainty, location (longitude and latitude), RGI7 ID, and feature code. Similarly, the proglacial lake inventory contains 9 attribute fields (Table 3), including a unique identifier, associated mountain range, type, mapping uncertainty, location (longitude and latitude), feature code, and a flag indicating whether the lake has disappeared. Both LTG and proglacial lake datasets include data for two time periods: 1990 and 2022, with identical attributes for both periods. The unique identifier is an automatically generated sequential integer, while the feature code follows the formats GmmmmmEnnnnnN (Feature_ID) for glaciers and GLmmmmmmEnnnnnN (Feature_ID) for lakes, where G denotes glacier, GL denotes glacier lake, m and n represent the longitude and latitude multiplied by 1000, respectively, and E and N indicate east longitude and north latitude. Identical LTGs and proglacial lakes share the same feature code (Feature_ID) to facilitate data linkage. Area and perimeter are calculated automatically from the feature geometry. The type of classification follows the criteria described in Section 3.2. Each feature's associated mountain range is determined by overlaying with mountain range boundaries, and mapping uncertainty is estimated according to Section 3.3.





Table 2 Attributes of the glacier dataset

Filed name	Type	Description
UID	Object ID	Unique code (Number)
Type	String	The classification of glaciers based on the relationship of interaction between glaciers and glacial lakes (Table 1)
Mountain	String	Mountain name where the glaciers is in
Area	Double	Area of glacier coverage(km²)
Error	Double	Area uncertainty of glacier mapping(km²)
Latitude	String	Latitude of the centroid of glacier
Longitude	String	Longitude of the centroid of glacier
rgi_id	String	RGI 7.0 id
Feature _ID	String	GmmmmmEnnnnN

186 187

Table 3 Attributes of the proglacial lake dataset

Filed name	Type	Description
UID	Object ID	Unique code (Number)
Туре	String	The classification of glacial lakes based on the relationship of interaction between glaciers and glacial lakes (Table 1)
Mountain	String	Mountain name where the glacial lake is in
Area	Double	Area of glacial lake coverage (km²)
Error	Double	Area uncertainty of glacial lake mapping (km²)
Latitude	String	Latitude of the centroid of glacier
Longitude	String	Longitude of the centroid of glacier
Disappear	String	Whether the proglacial lake disappeared in 2022 (Y)
Feature _ID	String	GLmmmmmEnnnnnN



4 Results

189

190

191

192

193

194

195

196

197

198

199

200

201

202

203

204

205

206

207

208

209

210

211

212

213

214

215

216

4.1 Spatial distribution of LTGs and proglacial lakes

Based on the changes in glacier-proglacial lake contact relationships from 1990 to 2022, glaciers were classified into three types (Table 1). Among them, Type 1 and Type 2 glaciers remained in contact with proglacial lakes from 1990 to 2022 and are therefore defined as LTGs. In contrast, Type 3 glaciers had become disconnected from proglacial lakes by 2022. Accordingly, only Type 1 and Type 2 glaciers were included when analyzing the distribution and extent of LTGs in 2022. In 2022, a total of 1740 LTGs were identified, with a combined area of 5082.08 ± 13.15 km². Concurrently, 1768 proglacial lakes were detected, with a total area of 262.10 ± 0.89 km². The discrepancy between glacier and lake counts stems from multi-lake associations per glacier and multi-glacier lakes were associated with two glaciers, and two lakes were in contact with three glaciers. The spatial distribution of LTGs in HMA shows marked heterogeneity (Figure 3). Predominantly concentrated along the southern margin, including the Himalayas, Nyainqentanglha, Gangdise Mountains, and Hindu Kush, these glaciers total 994, representing 57.13% of the study population (Figure 3b, Table A 1). The Central Himalaya hosts the highest number, with 232 glaciers (Table A 1), while the Nyainqentanglha accounts for the largest total glacier area $(1,001.05 \pm 3.32 \text{ km}^2,\text{Figure 3c})$. Glaciers were classified into nine size categories, ranging from $<0.05~km^2$ to $>100~km^2$ (Table A2). Among these, 1,095 glaciers (62.93%) are smaller than 1 km², covering 399.05 ± 1.07 km² (7.85% of the total area), while 93 glaciers (5.35%) exceed 10 km², covering 2964.68 ± 4.85 km² (58.34%). Only three glaciers exceed 100 km², spanning 785.42 ± 10.96 km². LTGs in HMA span elevations from 2,735 to 8,016 m, with a mean elevation of 5074 m (Figure 4). They are primarily concentrated between 5,000 and 6,000 m, where their combined area reaches 3030.2 ± 5.72 km² (59.52% of the total glacier area). Regional variations in elevation distribution are evident (Figure 4). In the Central Himalaya, Eastern Himalaya, Gangdise Mountains, Tibetan Interior Mountains, and Western Kunlun Shan, glacier area peaks occur around 6000 meters. Proglacial lakes in HMA are predominantly concentrated along the southern margin, with 1010 lakes (57.09%) in the Himalayas, Nyainqentanglha, Gangdise Mountains, and Hindu Kush (Table A 3). The Central Himalayas host the most lakes (240), with the largest total area (86.91 \pm 0.54 km², Figure 3 e). Proglacial lakes were grouped into five size categories (<0.05 to >1 km², Table A 4). Lakes smaller



than 0.1 km² are the most abundant, totaling 1384 (78.28%) and covering a combined area of 47.12 \pm
$0.30\ km^2$. Proglacial lakes in HMA span elevations from 2684 to 6012 m, with most concentrated
between 5000 and 5700 m, where 748 lakes (42.34%) cover 106.46 ± 0.59 km². Regional variations in
elevation distribution are evident (Figure 5). Gangdise Mountains and Western Kunlun Shan, proglacial
$lake \ numbers \ and \ areas \ peak \ around \ 5700 \ m. \ Conversely, in the Hindu Kush, Nyainqentanglha, Tanggulanglang, Tanggulanglang, Tanggulang, Tanggulan$
Shan, and Western Kunlun Shan, peak lake areas occur at lower elevations than peak lake numbers
(Figure 5).
Significant variations exist in the number and area distributions among glacier types in HMA. From
1990 to 2022, Type 2 glaciers, those forming new proglacial lakes, were the most numerous (1073, Table
A 1), dominating in all regions except Altun Shan/Eastern Kunlun Shan, Qilian Shan, and Tanggula Shan.
Conversely, Type 1 glaciers have the largest total area (3454.59 \pm 12.43 km²), concentrated primarily
in the Himalayas, Nyainqentanglha, Central Tien Shan, Qilian Shan, Tanggula Shan, and Western Kunlun
Shan (Table A 1). The Central Himalaya host the most glaciers across all types: 94 Type 1 (552.77 ±2.71
km²), 138 Type 2 (244.80 \pm 1.56 km²), and 84 Type 3 (202.67 \pm 1.11 km²). All glacier types show
consistent area peaks between $5,000$ and $6,000$ m, with similar patterns across subregions (Figure 4). In
$2022, Type\ 2\ proglacial\ lakes\ were\ the\ most\ numerous\ in\ HMA\ (1123, {\color{red}{\bf Table}}\ {\color{blue}{\bf A3}}), dominating\ in\ number\ {\color{blue}{\bf B3}}$
$across\ all\ regions\ except\ Altun\ Shan/Eastern\ Kunlun\ Shan,\ Qilian\ Shan,\ Karakoram,\ and\ Western\ Kunlun\ Shan,\ Gandard Shan,\ Ga$
Shan. Conversely, Type 1 lakes had the largest total area (207.18 \pm 0.82 km²) and accounted for the
largest share of total area in all regions except the Western Pamir, Hengduan Shan, Dzhungarsky Alatau,
and Eastern Tibetan Mountains. The central Himalaya hosted the greatest abundance of all three lake
types, with 91 Type 1 (76.89 \pm 0.51 km²), 149 Type 2, and 80 Type 3 (15.70 \pm 0.21 km²) lakes. The
Eastern Himalaya had the largest Type 2 lake area (10.73 \pm 0.03 km², Table A3). In HMA, the elevation
distribution of proglacial lake types is generally consistent, with peak numbers between 5000 and 5700
m and peak areas between 4700 and 5400 m (Figure 5). However, regional variations are observed in the
elevation distribution of lake numbers for different lake types. Specifically, in the Nyainqentanglha
$region, Type\ 2\ proglacial\ lakes\ exhibit\ a\ higher\ peak\ number\ range,\ between\ 5200\ and\ 5400\ m.\ Regarding$
area-elevation patterns, certain subregions display lower peak elevations, encompassing Type 2 lakes in





245	Kush, Nyainqentanglha, and Tanggula Shan (Figure 4).
246	4.2 Temporal changes in LTGs and proglacial lakes
247	From 1990 to 2022, glacier size has been continuously shrinking (Figure 3d). The total
248	area of all glacier types decreased by approximately 324.43 \pm 19.22 km², with Type 1 glaciers
249	experiencing the largest absolute loss of $137.46 \pm 17.62 \; km^2$, accounting for 42.37% of the total
250	reduction (Table A 5). The Central Himalay showed the most pronounced absolute area loss,
251	with a decrease of $74.46 \pm 3.46 \; km^2$, while the Hengduan Shan exhibited the highest relative
252	shrinkage at 16.42%. The Central Himalaya also recorded the largest absolute losses for all
253	three glacier types, with reductions of $37.20\pm3.91~km^2$ for Type 1, $20.13\pm2.26~km^2$ for Type
254	2, and 17.13 \pm 1.62 km^2 for Type 3 glaciers. In contrast, the Hengduan Shan had the highest
255	relative losses for all three types, at 25.34%, 13.95%, and 17.37%, respectively (Table A 5).
256	Small glaciers ($<$ 0.5 km 2) exhibited a significant increase in number, particularly those
257	smaller than 0.05 km², which grew by 51 in count with a total area increase of 1.68 \pm 0.08 km
258	2 (Table A 6). In contrast, glaciers in the $0.5-50~\mathrm{km^2}$ range showed a declining trend in number.
259	Among them, glaciers sized 0.5-1 km² experienced the largest numerical decrease (-57) and
260	the greatest relative area loss (-13.56%), while those in the $1-5~\mathrm{km^2}$ range incurred the most
261	substantial absolute area reduction, losing $97.17 \pm 3.5 \text{ km}^2$ (Table A 6).
262	Among the different glacier types, Type 1 glaciers experienced the greatest absolute area
263	loss, decreasing by 137.46 \pm 17.62 km ² (Table A 5). However, their relative area reduction of
264	3.83% was the smallest among the three types. By size class (Table A 6), Type 1 glaciers showed
265	the largest loss (63.39 \pm 6.38 km²) in the 10–50 km² range; Type 2 glaciers experienced the
266	greatest reduction (52.52 \pm 2.21 km²) in the 1–5 km² range. Type 3 glaciers showed the most
267	significant loss (27.51 \pm 1.57 km²) in the 5–10 km² range. For all three types, the 0.5–1 km²
268	size class exhibited the highest relative area reduction, at 9.06%, 15.37%, and 15.15%,
269	respectively.
270	Between 1990 and 2022, the total area of proglacial lakes increased by $138.19 \pm 1.18 \ km^2$,
271	representing a 62.09% expansion (Figure 3f and Table A2). The Central Himalaya experienced

the Eastern Himalaya and Northern Tibetan Mountains, and Type 1 lakes in the Eastern Pamirs, Hindu



272	the most significant absolute growth, with an increase of 42.32 ± 0.72 km² (70.19%), while the
273	Western Pamirs recorded the fastest relative growth, surging by 210.24%. The Central
274	Himalaya also saw the largest area increases across all three glacier types, with growth of 30.42
275	$\pm~0.64~km^2$ for Type 1 lakes, $10.02\pm0.16~km^2$ for Type 2, and $1.88\pm0.29~km^2$ for Type 3.
276	Regionally, the Dzhungarsky Alatau had the highest proportional increase in Type 1 lake area
277	at 176.38%, whereas the Eastern Himalaya recorded the largest proportional growth for Type 3 $$
278	lakes at 29.48% (Table A7).
279	During the study period, 1123 new proglacial lakes formed, while 25 lakes disappeared.
280	The number of small proglacial lakes (<0.5 km²) increased significantly, especially those
281	smaller than 0.05 km², which increased by 702 and accounted for 64.11% of the total increase
282	in lake numbers (Table A 8). Lakes larger than 1 km² contributed the largest increase in area
283	(60.44 \pm 0.81 km²), accounting for 43.74% of the total area growth. Moreover, lakes smaller
284	than 0.05 km² had the highest proportional area growth at 114.49%. Type 1 proglacial lakes
285	exhibited the most significant area growth, reaching 79.36 \pm 1.02 km², with a growth rate of
286	62.09% . Among size categories, the number of Type 1 lakes increased most in the $0.05-0.1~\mathrm{km}$
287	² range, with 49 new lakes added, while lakes larger than 1 km ² showed the greatest area
288	increase at $52.07 \pm 0.79 \text{ km}^2$ and the highest proportional growth at 85.19% .



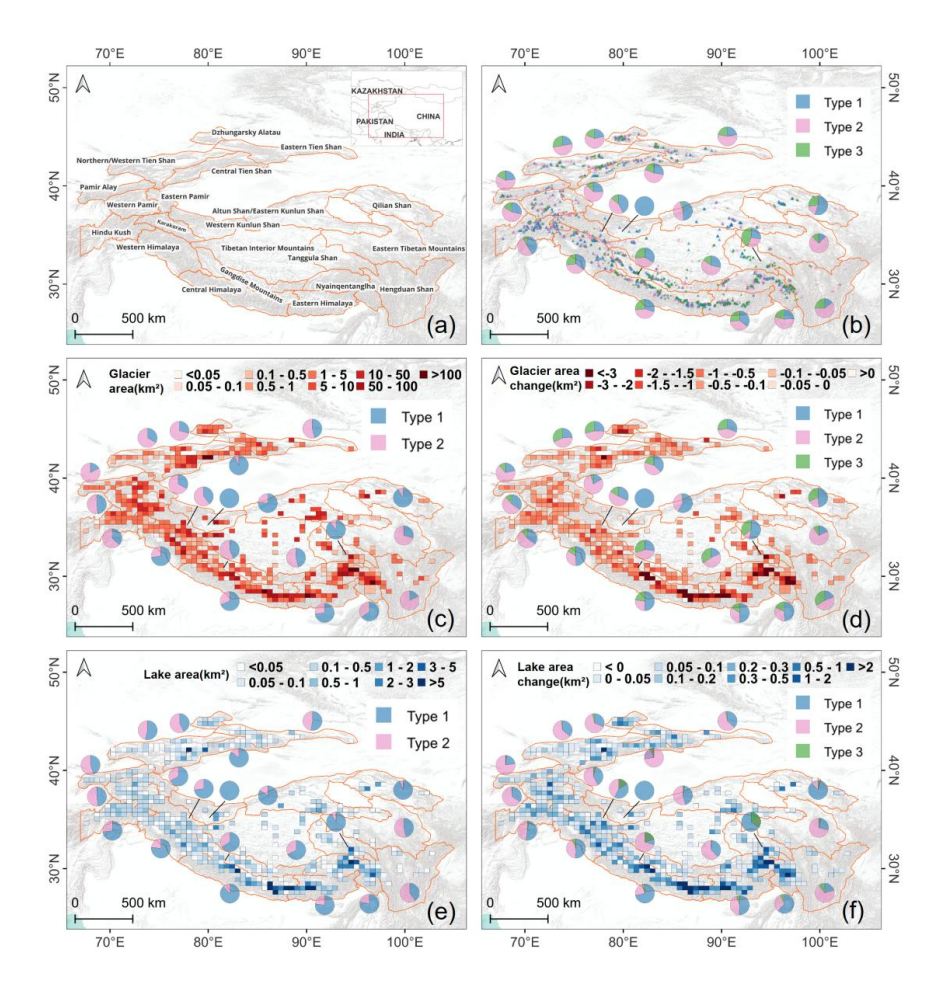


Figure 3: (a) Geographic extent of the mountain ranges in HMA. (b) Distribution of the three types of LTGs in 2022 and their numerical proportions across mountain regions. (c) Size distribution (Types 1 and 2) in 2022 and their area proportions. (d) Area changes of the three types of glaciers from 1990 to 2022 and their area-change proportions across mountain regions. (e) Area distribution of proglacial lakes (associated with Types 1 and 2 glaciers) in 2022 and their area proportions across mountain regions. (f) Area changes of the three types of proglacial lakes from 1990 to 2022 and their area-change proportions across mountain regions.

299

300 301





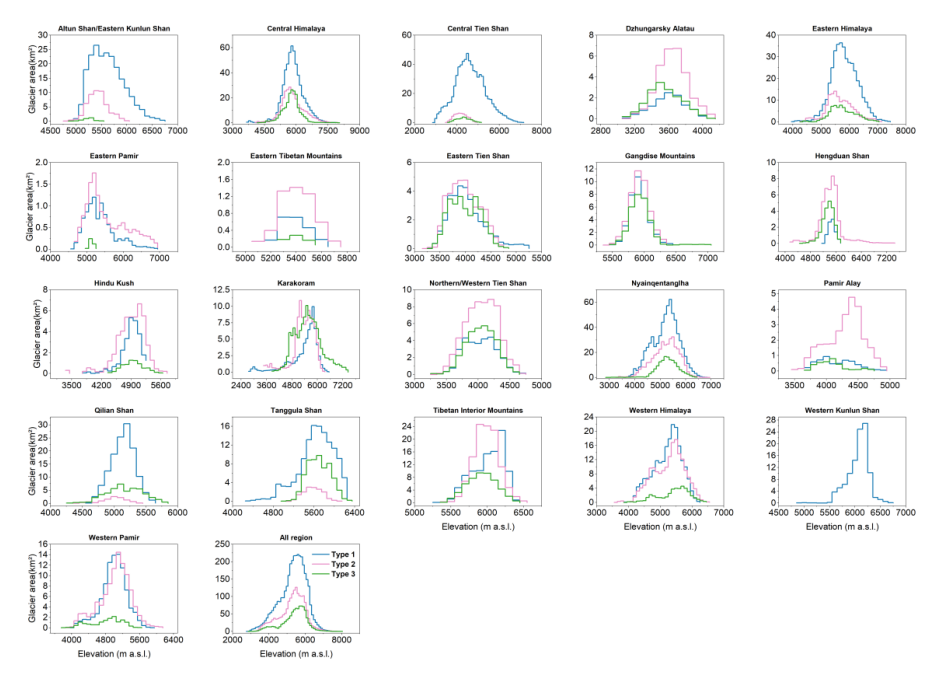


Figure 4: Area-Elevation distribution of LTGs across subregions, showing glacier area within 100 m elevation bins.

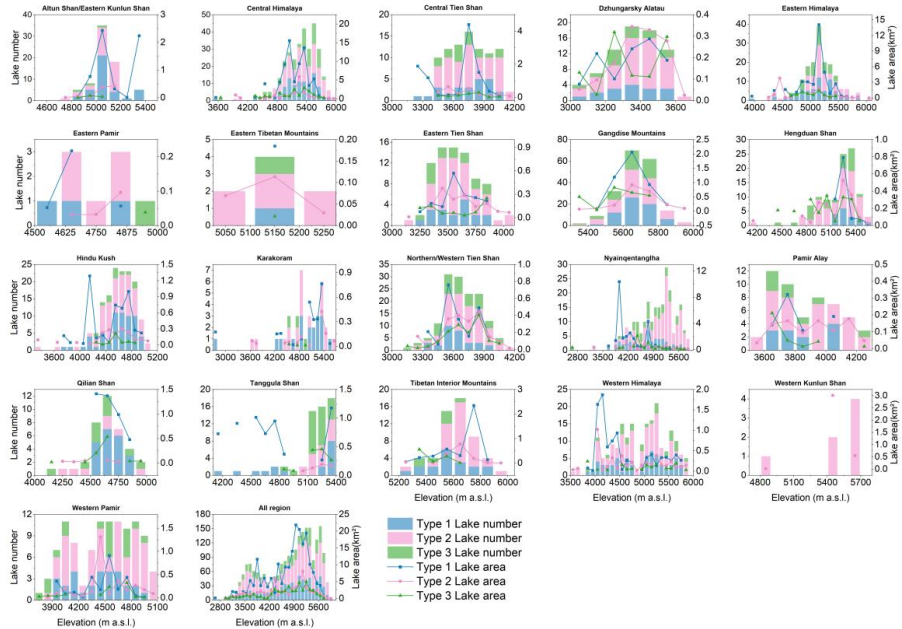


Figure 5 Distribution of proglacial lake numbers and areas across elevation ranges in each subregion. The number and area of proglacial lakes are presented within 100 m elevation bins for each subregion.



5 Discussion

5.1 Assessment of accuracy and errors

The uncertainty estimates indicate that as the glacier or lake area increases, the relative error of individual features decreases. In the study area, the total absolute area error for glaciers in 1990 and 2022 were $\pm 13.65 \,\mathrm{km^2}$ and $\pm 13.53 \,\mathrm{km^2}$, respectively, with average relative errors of $\pm 7.24\%$ and $\pm 8.12\%$. The relative error of glacier area shows a significant power-law relationship with the glacier size ($y = 0.056 \times x^{-0.427}$, $R^2 = 0.92$, Figure 6a). Additionally, the total absolute area error for proglacial lakes in 1990 and 2022 were $\pm 0.69 \,\mathrm{km^2}$ and $\pm 0.96 \,\mathrm{km^2}$, respectively, with average relative errors of $\pm 21.99\%$ and $\pm 23.69\%$, following a similar significant power-law relationship ($y = 0.050 \times x^{-0.463}$, $R^2 = 0.94$,



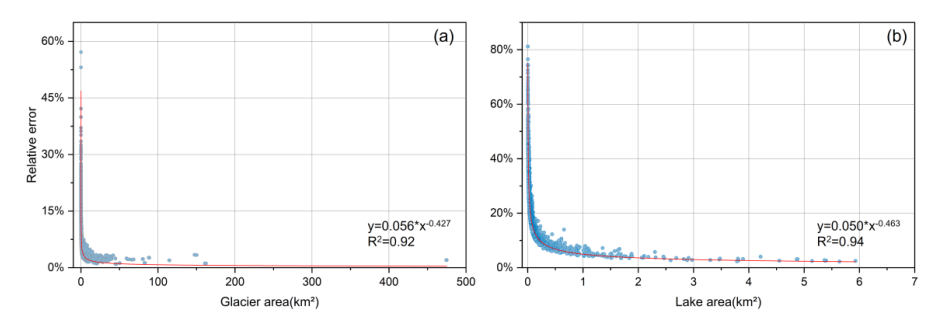


Figure 6: Estimation of relative errors for glaciers and proglacial lakes in the study area. (a) Glaciers (b) Proglacial lakes

5.2 Comparison and limitations

Publicly available data on LTGs and their proglacial lakes in HMA remain scarce, with recent datasets primarily focusing on glacial lakes. Consequently, this study selected two glacial lake datasets that partially overlap in time with our research and include proglacial lakes for comparison (Table 4). The results indicate that, within the same study area, our data closely align with those of Zhang et al. (2023). In 1990, the overlap rate of proglacial lakes between the dataset of Zhang et al. (2023) and ours exceeded 90%, while in 2020/2022, the overlap rate was 79%. In contrast, significant discrepancies were observed with the dataset of Chen et al. (2021). For the period 2017/2022, the dataset of Chen et al. (2021) identified 7850 proglacial lakes, whereas our study identified only 1,768, with an overlap rate of 67.82%. Through examining these datasets, we attribute these differences to variations in the identification of glacier-proglacial lake contact. Our study employs strict classification criteria (see Section 3.2), which

328

329

330

331

332

333

334

335

336

337

338

339

340

341

342

343

344

345

346

347

348

349

350

351

352

353

dynamics.





are reflected in three key aspects: (1) the lake must be located at the forefront of the glacier's flow direction; (2) a comprehensive evaluation of the glacier-lake contact surface based on the spatiotemporal evolution of both lake and glacier surface morphology; and (3) exclusion of ambiguous cases to ensure classification reliability. Additional factors, such as image quality, acquisition dates, and vectorization workflows, may also contribute to the observed discrepancies. A global inventory of LTGs was released in 2025 (Steiner et al., 2025). This dataset was derived from the RGI7 glacier outlines, primarily using Landsat 5-7 TM/ETM+ imagery (ca. 1998-2002), supplemented by ASTER data in some high-latitude regions. Existing regional proglacial lake inventories (when close to 2000) were also incorporated, and the identification of LTGs was conducted through manual interpretation and expert cross-validation. Based on the degree of glacier-lake contact, glaciers were classified into four types. In HMA, a total of 1912 LTGs were identified. Although the glacier termini in this dataset were delineated for 2000 ± 2 , the overlap with our 2022 dataset is 47.4%. Given that our results indicate that glacier-lake contact is not always stable, differences in the timing of terminus delineation are likely the primary source of the observed discrepancies. Although this study employed standardized criteria for the qualitative identification of LTGs and their proglacial lakes, subjective factors remain challenging to eliminate entirely during remote sensing imagery analysis. Differences in how analysts interpret imagery, apply calibration standards, and process data quality directly impact the results. While measures such as independent labeling and cross-validation by multiple analysts can reduce subjective bias, uncertainties stemming from variations in individual experience, judgment criteria, and image quality remain difficult to fully resolve. Consequently, further quantification of identification criteria is of paramount importance. In the future, more refined technical approaches can optimize the identification of glacier-lake contact lines, leveraging high-resolution imagery and automated analysis tools to enhance accuracy. Additionally, quantifying the depth of glaciers within lakes will provide more precise data support. These quantitative standards not only effectively minimize human-induced variability but also significantly improve the precision of glacier-lake contact relationship assessments, laying a more reliable data foundation for subsequent studies of glacier





Table 4: Comparisons of glacial lake mapping in this study with previous studies for the similar extended region.

Year (previous/this study)	Region	Area threshod (km²)	Source	Count (Area/km²) Previous studies	Count (Area/km²) This study	Overlap count
1990/1990	0		(7)	651(129.76±0.89)	645(122.08±0.59)	615(95.35%)
2020/2022	Greater Himalaya	0.0036	(Zhang et al., 2023)	1115(192.42±1.23)	1029 (199.83±0.79)	841(79.11%)
2017/2022	НМА	0.0081	(Chen et al., 2021)	7850(684.62±10.06)	1768(262.03±0.89)	1199(67.82%)

6 Conclusions

Using Landsat imagery, we applied a semi-automated mapping approach in Google Earth Engine (GEE) to inventory proglacial lakes across High Mountain Asia (HMA) in the 1990s and 2020s, and compiled the first region-wide dataset of LTGs and their proglacial lakes. In 2022, HMA contained 1740 LTGs (5082.08 \pm 13.15 km²), of which 667 glaciers (3454.59 \pm 12.43 km²) maintained lake contact since 1990, and 1073 glaciers (1,627.49 \pm 4.30 km²) developed new proglacial lakes. These glaciers were mainly distributed between 2735 and 8016 m a.s.l. Additionally, 468 glaciers (960.13 \pm 3.18 km²) lost lake contact during the period.

A total of 1768 proglacial lakes (262.10 \pm 0.89 km²) were connected to glaciers in 2022, including 645 lakes (207.18 \pm 0.82 km²) with continuous glacier contact and 1123 newly formed lakes (54.85 \pm 0.35 km²). Lakes were mainly distributed between 2684 and 6012 m a.s.l. Meanwhile, 485 lakes (45.31 \pm 0.34 km²) lost glacier contact, with 25 disappearing entirely. From 1990 to 2022, LTGs retreated by 324.43 \pm 19.23 km² (–5.1%), while proglacial lake area increased by 138.19 \pm 1.18 km² (+81.7%). The development and evolution of lake-terminating glacier–proglacial lake systems are predominantly concentrated along the southern margin of HMA, including the Hindu Kush, Himalayas, Nyainqentanglha, and Gangdise Mountains.

This dataset offers a robust basis for examining spatially heterogeneous glacier responses to climate change, coupled glacier-lake evolution, glacier hydrological modeling, glacial lake outburst flood (GLOF) assessment, and water resource management. Nevertheless, further improvements in data quality

https://doi.org/10.5194/essd-2025-596 Preprint. Discussion started: 20 October 2025 © Author(s) 2025. CC BY 4.0 License.





376	remain necessary, particularly in quantifying glacier-lake contact line length, the degree of glacier-lake
377	contact (e.g., lake depth and subaqueous glacier front depth), and water temperature measurements.
378	
379	Financial support. This work was funded by the National Key R&D Program of China (Grant No.
380	2024YFC3013400) and National Science Foundation of China (Grant No. 42361144874).
381	
382	$\textbf{Author contributions.} \ YL \ designed \ the \ study, \ developed \ the \ methodology, \ performed \ analysis, \ and$
383	$wrote the \ manuscript. \ QL \ provided \ funding, \ support \ and \ supervision. \ XL, YY \ and \ JY \ produced \ data \ and$
384	performed analysis. All other authors discussed and drafted the formulation of the specifications of the
385	glacial lake inventory in this study. All authors contributed to the final form of the paper.
386	Competing interests. The authors declare that they have no conflict of interest.
387	
388	Code and data availability. Data described in this manuscript can be accessed at Zenodo under
389	$https://doi.org/10.5281/zenodo.17369580 \ (Luo \ and \ Liu, \ 2025). \ The \ code \ for \ proglacial \ lake \ ident$
390	$-ification\ can\ be\ accessed\ via\ https://code.earthengine.google.com/00573a1f3c8684d6f3e0722677f5$
391	4b64.
392	
393	

https://doi.org/10.5194/essd-2025-596 Preprint. Discussion started: 20 October 2025 © Author(s) 2025. CC BY 4.0 License.





Appendix A

Table A1 Glacier type statistics (number and area) across subregions





								Glacier area (km²)	a (km²)			
Region		Glacier number	in moet	1		1990s	s0			2022s	2s	
	Type 1	Type 2	Type 3	Total	Type 1	Type 2	Type 3	Total	Type 1	Type 2	Type 3	Total
Central Himalaya	94	138	84	316	589.97±2.81	264.93±1.64	219.8±1.17	1074.7±3.46	552.77±2.71	244.8±1.56	202.67±1.11	1000.25±3.32
Westem Himalaya	99	106	28	200	198.31±2.11	176.41±1.67	42.54±0.47	417.26±2.74	192.5±2.08	167.24±1.64	40.28±0.45	400.02±2.69
Eastern Himalaya	25	89	48	180	419.67±2.06	155.37±1.07	87.2±0.68	662.24±2.42	392.93±1.97	136.97±0.98	78.65±0.63	608.55±2.29
Gangdise Mountains	\$	77	50	161	35.19±0.32	45.65±0.37	33.34±0.33	114.17±0.59	31.79±0.31	40.11±0.34	29.53±0.31	101.44±0.55
Hindu Kush	61	75	12	148	26.49±0.31	45.82±0.41	8.71±0.17	81.02±0.54	23.58±0.29	41.34±0.39	7.83±0.16	72.74±0.51
Nyainqentanglha	55	126	48	229	677.08±3.76	368.21±2.96	164.46±1.28	1209.75±4.95	650.54±3.73	350.51±2.91	154.73±1.22	1155.78±4.89
Altun Shan/Eastern Kunlun Shan	32	30	3	9	197.95±0.85	62.54±0.42	4.09±0.09	264.59±0.95	194.08±0.84	59.98±0.41	3.95±0.09	258.02±0.93
Northem/Western Tien Shan	32	73	40	145	31.78±0.37	63.81±0.53	37.44±0.35	133.03±0.74	28.79±0.35	58.39±0.51	33.45±0.33	120.63±0.7
Western Pamir	30	59	17	901	93.74±0.95	99.99±0.84	16.58±0.29	210.3±1.09	89.95±0.93	94.04±0.8	15.33±0.28	199.33±1.26
Central Tien Shan	25	49	17	16	733.67±10.9	53.48±0.64	29.86±0.6	817.01±10.94	729.83±10.9	49.1±0.61	27.78±0.57	806.71±10.93
Qilian Shan	21	7	10	38	119.22±0.92	11.38±0.19	59.35±0.54	189.95±1.08	116.6±0.9	10.31±0.18	57.66±0.52	184.57±1.05
Eastern Tien Shan	18	46	118	82	33.23±0.54	39.06±0.38	29.91±0.54	102.2±0.85	30.49±0.52	35.32±0.36	27.46±0.52	93.27±0.82
Karakoram	18	18	9	42	66.51±0.78	102.9±0.99	128.82±2.25	298.24±2.58	65.1±0.76	100.62±0.97	128.1±2.25	293.82±2.56
Tanggula Shan	17	17	27	19	130.26±0.94	14.97±0.24	62.7±0.54	207.93±1.11	124.33±0.91	13.75±0.23	58.63±0.52	196.7±1.07
Tibetan Interior Mountains	17	34	6	09	96.32±0.72	112.16±0.74	53.53±0.49	262.02±1.14	95.32±0.71	109.47±0.73	51.62±0.46	256.4±1.12
Dzhungarsky Alatau	16	45	14	75	12.85±0.2	32.15±0.31	17.71±0.26	62.71±0.45	10.78±0.18	28.49±0.29	15.41±0.24	54.68±0.42
Hengduan Shan	16	99	27	108	10.75±0.18	49.63±0.5	27.82±0.31	88.2±0.61	8.03±0.16	42.71±0.47	22.99±0.27	73.72±0.57
Pamir Alay	Ξ	29	∞	48	5.79±0.12	27.8±0.38	3.42±0.11	37±0.42	5.12±0.12	25.74±0.37	3.05 ± 0.11	33.91 ± 0.4
Western Kunlun Shan	7	0	0	7	104.03±1.08	0	0	104.03±1.08	103.14±1.08	0	0	103.14±1.08
Eastem Pamir	2	5	1	∞	6.89±0.22	14.14±0.28	0.39±0.03	21.43±0.35	6.82±0.21	13.78±0.27	0.37±0.03	20.97±0.35
Eastern Tibetan Mountains	-	9	-	∞	2.35±0.08	5.75±0.14	0.76±0.05	8.86±0.16	2.12±0.08	4.83±0.14	0.64±0.04	7.59±0.16
Total	299	1073	468	2208	3592.05±12.49	1746.17±4.43	1028.43±3.28	6366.64±13.65	3454.59±12.43	1627.49±4.3	960.13±3.18	6042.24±13.53





	J	Glacier number (1990s)	er (1990s)		ซี	Glacier number (2022s)	er (2022s)			Glacier area (km²)(1990s)	(km²)(1990s)			Glacier area (km²)(2022s)	(km²)(2022s)	
Glacier size (km²)	Type 1	Type 1 Type 2 Type 3	Type 3	Total	Type 1	Type 2	Type 3	Total	Type 1	Type 2	Type 3	Total	Type 1	Type 2	Type 3	Total
<0.05	∞	6	4	21	20	33	19	72	0.31±0.03	0.33±0.03	0.15±0.02	0.78±0.04	0.72±0.04	1.05±0.05	0.69±0.04	2.46±0.07
0.05-0.1	28	43	26	76	37	72	28	137	2.22±0.07	3.24±0.08	1.86±0.06	7.32±0.12	2.72±0.08	5.36±0.11	2.07±0.06	10.15±0.15
0.1-0.5	991	437	136	739	168	442	151	761	44.18±0.34	118.86±0.54	39.44±0.31	202.48±0.71	45.06±0.34	118.54±0.54	43.13±0.33	206.73±0.72
0.5-1	126	239	101	466	118	205	98	409	92.8±0.53	166.86±0.72	71.75±0.47	331.41±1.01	84.4±0.52	141.21±0.66	60.88±0.44	286.49±0.94
1-5	197	277	154	829	188	256	141	285	478.95±1.49	563.75±1.61	343.68±1.24	1386.38±2.52	459.59±1.47	515.28±1.55	318.5±1.18	1289.21±2.44
5-10	71	43	30	4	29	14	26	134	498.24±1.92	303.8±1.57	207.84±1.19	1009.87±2.75	455.09±1.82	287.6±1.51	180.33±1.09	927.97±2.56
10-50	63	23	16	102	19	22	16	66	1347.15±4.57	432.18±2.45	248.78±1.6	2028.11±5.43	1268.56±4.37	432.17±2.49	240.09±1.54	1931.43±5.26
50-100	S	2	0	7	S	2	0	7	343.42±2.96	157.16±2.78	0	500.58±4.06	332.14±2.97	155.79±2.76	0	487.93±4.05
>100	3	0	-	4	3	0	-	4	784.78±10.96	0	114.93±2.23	899.7±11.18	785.42±10.96	0	114.44±2.22	899.86±11.18
Total	299	1073	468	2208	299	1073	468	2208	3592.05±12.49	1746.17±4.43	1028.43±3.28	6366.64±13.65	3454.59±12.43	1627.49±4.3	960.13±3.18	6042.24±13.53





		Lake number (1990s)	er (1990s)		T	Lake number (2022s)	er (2022s)			Lake area	Lake area (km²) (1990s)			Lake area (l	Lake area (km²) (2022s)	
Kegion	Type 1	Type 2	Type 3	Total	Type 1	Type 2	Type 3	Total	Type 1	Type 2	Type 3	Total	Type 1	Type 2	Type 3	Total
Central Himalaya	91	0	98	177	91	149	80	320	46.47±0.38	0	13.83±0.2	60.29±0.43	76.89±0.51	10.02±0.16	15.7±0.21	102.62±0.58
Western Himalaya	92	0	28	93	9	107	27	199	4.17±0.11	0	1.2±0.05	5.38±0.12	9.02±0.15	4.13±0.09	1.51±0.06	14.66±0.19
Eastern Himalaya	57	0	90	107	99	75	49	180	23.92±0.26	0	5.05±0.11	28.98±0.29	36.75±0.36	10.89±0.18	6.55±0.13	54.19±0.42
Gangdise Mountains	99	0	51	116	99	79	51	195	3.72±0.1	0	3.19±0.08	6.91 ± 0.13	4.49±0.1	2.32±0.07	2.67±0.07	9.48±0.14
Hindu Kush	09	0	12	72	19	75	12	148	2.97±0.08	0	0.61 ± 0.04	3.58±0.09	4.83±0.11	1.81 ± 0.06	0.49±0.04	7.13±0.12
Nyainqentanglha	52	0	51	103	52	135	49	236	12.53±0.18	0	5.78±0.13	18.31±0.22	28.57±0.3	8.16±0.14	7.52±0.14	44.25±0.36
Altun Shan/Eastern Kunlun Shan	33	0	3	36	32	38	3	73	4.83±0.14	0	0.17±0.02	5±0.14	5.68±0.14	1.06±0.05	0.11±0.02	6.85±0.15
Northem/Western Tien Shan	32	0	41	73	31	75	39	145	1.15±0.05	0	1.44±0.05	2.6±0.07	2.3±0.07	1.97±0.06	1.51±0.06	5.77±0.11
Western Pamir	28	0	19	47	28	09	19	107	1.27±0.05	0	0.91 ± 0.04	2.17±0.07	2.81 ± 0.08	3.04±0.08	0.89±0.04	6.74±0.12
Central Tien Shan	26	0	17	43	25	49	16	06	10.78 ± 0.17	0	0.71 ± 0.04	11.49±0.18	10.37±0.21	1.81±0.06	0.81 ± 0.04	13±0.22
Qilian Shan	20	0	Ξ	31	20	∞	Ξ	39	2.81±0.07	0	0.95 ± 0.04	3.76±0.09	4.24±0.1	0.26±0.02	0.88 ± 0.04	5.37±0.11
Eastern Tien Shan	17	0	20	37	17	47	16	80	0.76±0.04	0	0.73 ± 0.04	1.49 ± 0.05	1.72±0.06	1.56±0.05	0.8 ± 0.04	4.08±0.09
Karakoram	19	0	S	24	19	17	3	39	1.69±0.07	0	0.32 ± 0.03	2.02 ± 0.07	2.64±0.08	0.98±0.04	0.05±0.01	3.66±0.09
Tanggula Shan	17	0	28	45	17	17	26	09	3.1 ± 0.08	0	2.28±0.09	5.38±0.12	6.15±0.12	0.57±0.03	1.35±0.05	8.07±0.14
Tibetan Interior Mountains	4	0	6	23	14	35	7	99	2.56±0.11	0	0.94 ± 0.05	3.5±0.12	3.58 ± 0.14	1.75±0.06	0.91 ± 0.04	6.23±0.16
Dzhungarsky Alatau	14	0	16	30	41	84	15	77	0.37±0.03	0	1.17 ± 0.05	1.54 ± 0.06	1.03 ± 0.05	1.38±0.05	1.25±0.05	3.66±0.09
Hengduan Shan	15	0	28	43	15	99	27	108	0.71±0.04	0	1.63±0.06	2.35±0.07	1.26±0.06	1.84±0.06	1.91±0.07	5.01±0.11
Pamir Alay	12	0	∞	20	12	32	∞	52	0.5 ± 0.03	0	0.34 ± 0.02	0.84 ± 0.02	0.77±0.04	0.94±0.04	0.33±0.02	2.03±0.05
Western Kunlun Shan	7	0	0	7	7	0	0	7	3.17±0.08	0	0	3.17 ± 0.08	3.59±0.09	0	0	3.59 ± 0.09
Eastem Pamir	ю	0	-	4	ю	5	-	6	0.22 ± 0.03	0	0.05 ± 0.01	0.26 ± 0.03	0.33±0.02	0.16 ± 0.02	0.04 ± 0.01	0.53 ± 0.03
Eastem Tibetan Mountains	-	0	-	7	-	9	-	œ	0.1 ± 0.01	0	0.04 ± 0.01	0.14 ± 0.02	0.19 ± 0.02	0.21 ± 0.02	0.02 ± 0.01	0.42 ± 0.03
Total	648	0	485	1133	645	1123	460	2228	127.82±0.61	0	41.33±0.32	169.15±0.69	207.18±0.82	54.85±0.35	45.31±0.34	307.34±0.96





				Lake number	ımper							Lake area (km²)	2a (km²)			
Glacier size (km²)		1990s	0s			2022s	2s			19	1990s			2022s	22s	
	Type 1	Type 2	Type 3	Total	Type 1	Type 2	Type 3	Total	Type 1	Type 2	Type 3	Total	Type 1	Type 2	Type 3	Total
<0.05	338	0	289	627	197	887	245	1329	7.62±0.12	0	7.5±0.12	7.5±0.12 15.12±0.16 5.71±0.11 20.58±0.19 6.13±0.11 32.42±0.25	5.71±0.11	20.58±0.19	6.13±0.11	32.42±0.25
0.05-0.1	96	0	93	189	145	155	92	392	6.58±0.12	0	6.45±0.12	645±0.12 13.03±0.17 10.02±0.15 10.81±0.15 6.56±0.12 27.39±0.24	10.02±0.15	10.81±0.15	6.56±0.12	27.39±0.24
0.1-0.5	157	0	06	247	204	72	111	387	32.46±0.28	0	17.77±0.21	17.77±0.21 50.24±0.34 47.07±0.35 13.19±0.17 23.25±0.24 83.51±0.46	47.07±0.35	13.19±0.17	23.25±0.24	83.51±0.46
0.5-1	30	0	12	45	47	9	6	62	20.03±0.25	0	8.44±0.17	8.44±0.17 28.47±0.3 31.18±0.32 4.43±0.14 5.67±0.13 41.28±0.37	31.18±0.32	4.43±0.14	5.67±0.13	41.28±0.37
~	27	0	-	28	52	ю	ю	28	61.12±0.45	0	1.17±0.06	1.17±0.06 62.29±0.45 113.19±0.65 5.84±0.12 3.7±0.12 122.73±0.67	113.19±0.65	5.84±0.12	3.7±0.12	122.73±0.67
Total	648	0	485	1133	645	1123	460	2228	2228 127.82±0.61	0	41.33±0.32	41.33±0.32 169.15±0.69 207.18±0.82 54.85±0.35 45.31±0.34 307.34±0.96	207.18±0.82	54.85±0.35	45.31±0.34	307.34±0.96





Table A.S. Artea changes of uniterent graciel types in each subregion (1770–1022)	0							
Dordon		Area loss(km²)	(km²)			Area loss(%)		
N cgross	Type 1	Type 2	Type 3	Total	Type 1	Type 2	Type 3	Total
Central Himalaya	37.2±3.91	20.13±2.26	17.13±1.62	74.46±4.8	6.31	7.6	7.79	6.93
Western Himalaya	5.81±2.97	9.17±2.34	2.26±0.65	17.24±3.84	2.93	5.2	5.31	4.13
Eastem Himalaya	26.74±2.85	18.41±1.45	8.55±0.93	53.7±3.33	6.37	11.85	8.6	8.11
Gangdise Mountains	3.39±0.44	5.54±0.5	3.8±0.46	12.73±0.81	9.65	12.14	11.41	11.16
Hindu Kush	2.91±0.43	4.48±0.56	0.88±0.23	8.27±0.74	10.98	9.78	10.13	10.21
Nyainqentanglha	26.54±5.29	17.7±4.15	9.72±1.77	53.96 ± 6.95	3.92	4.81	5.91	4.46
Altun Shan/Eastern Kunlun Shan	3.87±1.19	2.57±0.59	0.14±0.13	6.58±1.33	1.95	4.1	3.38	2.48
Northern/Westem Tien Shan	2.99±0.51	5.42±0.74	3.99±0.49	12.4±1.02	9.42	8.49	10.66	9.32
Westem Pamir	3.79±1.33	5.95±1.16	1.24±0.4	10.98±1.81	4.04	5.95	7.51	5.22
Central Tien Shan	3.84±15.42	4.38±0.88	2.08±0.83	10.3±15.47	0.52	8.19	26.9	1.26
Qilian Shan	2.62±1.28	1.07±0.27	1.7±0.75	5.39±1.51	2.2	9.4	2.86	2.84
Eastern Tien Shan	2.74±0.75	3.74±0.52	2.45±0.75	8.93±1.18	8.25	9.58	8.18	8.74
Karakoram	1.41±1.09	2.29±1.39	0.72±3.18	4.42±3.64	2.12	2.22	0.56	1.48
Tanggula Shan	5.94±1.31	1.22±0.33	4.07±0.75	11.23±1.55	4.56	8.18	6.49	5.4
Tibetan Interior Mountains	1.01±1.02	2.69±1.04	1.92±0.68	5.62±1.61	1.04	2.4	3.58	2.14
Dzhungarsky Alatau	2.07±0.26	3.66±0.43	2.3±0.36	8.03±0.62	16.1	11.38	12.99	12.8
Hengduan Shan	2.73±0.24	6.92±0.69	4.83±0.41	14.48±0.84	25.34	13.95	17.37	16.42
Pamir Alay	0.67±0.17	2.06±0.53	0.37±0.15	3.1 ± 0.58	11.55	7.4	10.75	8.36
Western Kunlun Shan	0.89±1.53	0	0	0.89±1.53	0.86	0	0	98.0
Eastern Pamir	0.08±0.3	0.36±0.39	0.02±0.04	0.46±0.49	1.1	2.57	5.37	2.15
Eastem Tibetan Mountains	0.23±0.11	0.92±0.19	0.12±0.06	1.27±0.23	9.81	15.94	16.33	14.35
Total	137.46±17.62	118.68±6.18	68.29±4.58	324.43±19.23	3.83	8.9	6.64	5.1





Glacier size		Number change(count)	count)			Area change(km²)	ıge(km²)			Area change(%)	nge(%)	
(km²)	Type 1	Type 2	Type 3	Total	Type 1	Type 2	Type 3	Total	Type 1	Type 2	Type 3	Total
<0.05	12	24	15	51	0.41±0.05	0.73±0.05	0.54±0.04	1.68±0.08	133.95	224.58	367.1	215.87
0.05-0.1	6	29	2	40	0.58±0.1	2.04±0.13	0.21±0.09	2.83±0.19	26.17	62.92	11.3	38.68
0.1-0.5	2	8	15	22	1.67±0.48	-1.1±0.77	3.68±0.46	4.25±1.02	3.78	-0.93	9.33	2.1
0.5-1	œ,	-34	-15	-57	-8.41±0.74	-25.65±0.97	-10.87±0.64	-44.93±1.38	-9.06	-15.37	-15.15	-13.56
1-5	6-	-21	-13	43	-19.48±2.11	-52.52±2.21	-25.17±1.71	-97.17±3.5	-4.07	-9.32	-7.32	-7.01
5-10	4	-2	4	-10	-38.2±2.62	-16.19±2.18	-27.51±1.57	-81.9±3.75	-7.67	-5.33	-13.24	-8.11
10-50	-2	7	0	٤-	-63.39±6.38	-24.61±3.4	-8.69±2.22	-96.69±7.56	-4.71	-5.69	-3.49	4.77
50-100	0	0	0	0	-11.28±4.19	-1.37±3.92	0	-12.65±5.74	-3.28	-0.87		-2.53
>100	0	0	0	0	0.64±15.5	0	-0.48±3.15	0.16±15.82	0.08		-0.42	0.02
Total	0	0	0	0	-137.46±17.62	-118.67±6.17	-68.29±4.57	-324.42±27.18	-3.83	8.9-	-6.64	-5.1

Table A 6 Area and number changes of three glacier types across different size classes



Table A 7 Area changes of different glacial lake types in each subregion (1990–2022)

		Area chan	ge (km²)		Area	a change (%	6)
Region	Type 1	Type 2	Type 3	Total	Type 1	Type 3	Total
Central Himalaya	30.42±0.64	10.02±0.16	1.88±0.29	42.32±0.72	65.46	13.6	70.19
Western Himalaya	4.84±0.19	4.13±0.09	0.31±0.07	9.28±0.22	115.95	25.8	172.62
Eastern Himalaya	12.83±0.45	10.89±0.18	1.49±0.17	25.22±0.51	53.63	29.49	87.04
Gangdise Mountains	0.77±0.14	2.32±0.07	-0.52±0.11	2.57±0.19	20.7	-16.32	37.21
Hindu Kush	1.86±0.13	1.81±0.06	-0.11±0.05	3.55±0.15	62.57	-18.1	99.15
Nyainqentanglha	16.04±0.35	8.16±0.14	1.74±0.19	25.95±0.42	128.03	30.11	141.75
Altun Shan/Eastern Kunlun Shan	0.85±0.2	1.06±0.05	-0.05±0.02	1.86±0.21	17.59	-30.3	37.21
Northern/Western Tien Shan	1.14±0.09	1.97±0.06	0.07±0.08	3.17±0.13	98.76	4.86	122.14
Western Pamir	1.54±0.09	3.04±0.08	-0.02±0.06	4.57±0.14	121.66	-2.2	210.24
Central Tien Shan	-0.41±0.27	1.81±0.06	0.11±0.06	1.51±0.28	-3.8	15.59	13.14
Qilian Shan	1.43±0.12	0.26±0.02	-0.07±0.06	1.61±0.14	50.93	-7.34	42.8
Eastern Tien Shan	0.96±0.08	1.56±0.05	0.07±0.06	2.59±0.11	126.23	9.62	174
Karakoram	0.94±0.11	0.98±0.04	-0.28±0.03	1.64±0.12	55.52	-86.41	81.3
Tanggula Shan	3.04±0.14	0.57±0.03	-0.93±0.1	2.69±0.18	98.01	-40.83	50
Tibetan Interior Mountains	1.02±0.18	1.75±0.06	-0.03±0.07	2.73±0.2	39.92	-3.18	78.03
Dzhungarsky Alatau	0.66±0.06	1.38±0.05	0.08±0.07	2.12±0.1	176.38	6.85	137.53
Hengduan Shan	0.55±0.07	1.84±0.06	0.28±0.09	2.66±0.13	76.97	17.13	113.23
Pamir Alay	0.27±0.05	0.94±0.04	-0.02±0.03	1.19±0.07	54.26	-5.82	141.49
Western Kunlun Shan	0.42±0.12	0	0	0.42±0.12	13.26		13.26
Eastern Pamir	0.11±0.04	0.16±0.02	-0.01±0.01	0.26±0.04	50.87	-20.66	98.25
Eastern Tibetan Mountains	0.08±0.02	0.21±0.02	-0.01±0.01	0.28±0.04	77.14	-27.51	199.92
Total	79.36±1.02	54.85±0.35	3.98±0.47	138.19±1.18	62.09	9.63	81.7

Table A 8 Area and number changes of proglacial lakes of three glacier types across different size classes

CI		Number	change			Area cha	inge(km²)		Are	ea change(%	6)
Glacier size (km²)	Type 1	Type 2	Type 3	Total	Type 1	Type 2	Type 3	Total	Type 1	Type 3	Total
<0.05	-141	887	-44	702	-1.91±0.16	20.58±0.19	-1.36±0.16	17.31±0.3	-25.07	-18.14	114.49
0.05-0.1	49	155	-1	203	3.44±0.19	10.81±0.15	0.11±0.17	14.36±0.29	52.27	1.71	110.23
0.1-0.5	47	72	21	140	14.61±0.44	13.19±0.17	5.47±0.32	33.27±0.57	45	30.77	66.22
0.5-1	17	6	-3	20	11.15±0.4	4.43±0.14	-2.76±0.21	12.82±0.48	55.66	-32.72	45.04
>1	25	3	2	30	52.07±0.79	5.84±0.12	2.53±0.13	60.44±0.81	85.19	215.49	97.02
Total	-3	1123	-25	1095	79.36±1.02	54.85±0.35	3.98±0.46	138.19±1.18	62.09	9.63	81.7





Reference

Benn, D. I., Hulton, N. R. J., and Mottram, R. H.: 'Calving laws', 'sliding laws' and the stability of tidewater glaciers, Ann Glaciol, 46, 123-130, 10.3189/172756407782871161, 2007a.

Benn, D. I., Warren, C. R., and Mottram, R. H.: Calving processes and the dynamics of calving glaciers, Earth-Science Reviews, 82, 143-179, 10.1016/j.earscirev.2007.02.002, 2007b.

Bolch, T., Menounos, B., and Wheate, R.: Landsat-based inventory of glaciers in western Canada, 1985–2005, Remote Sens Environ, 114, 127-137, https://doi.org/10.1016/j.rse.2009.08.015, 2010.

Brun, F., Berthier, E., Wagnon, P., Kaab, A., and Treichler, D.: A spatially resolved estimate of High Mountain Asia glacier mass balances, 2000-2016, Nat Geosci, 10, 668-673, 10.1038/NGEO2999, 2017.

Brun, F., Wagnon, P., Berthier, E., Jomelli, V., Maharjan, S. B., Shrestha, F., and Kraaijenbrink, P. D. A.: Heterogeneous Influence of Glacier Morphology on the Mass Balance Variability in High Mountain Asia, Journal of Geophysical Research: Earth Surface, 124, 1331-1345, 10.1029/2018jf004838, 2019.

Carrivick, J. L. and Tweed, F. S.: Proglacial lakes: character, behaviour and geological importance, Quaternary Sci Rev, 78, 34-52, 10.1016/j.quascirev.2013.07.028, 2013.

Chen, F., Zhang, M., Guo, H., Allen, S., Kargel, J. S., Haritashya, U. K., and Watson, C. S.: Annual 30 m dataset for glacial lakes in High Mountain Asia from 2008 to 2017, Earth System Science Data, 13, 741-766, 10.5194/essd-13-741-2021, 2021.

Chernos, M., Koppes, M., and Moore, R. D.: Ablation from calving and surface melt at lake-terminating Bridge Glacier, British Columbia, 1984–2013, The Cryosphere, 10, 87-102, 10.5194/tc-10-87-2016, 2016.

Foga, S., Scaramuzza, P. L., Guo, S., Zhu, Z., Dilley, R. D., Beckmann, T., Schmidt, G. L., Dwyer, J. L., Joseph Hughes, M., and Laue, B.: Cloud detection algorithm comparison and validation for operational Landsat data products, Remote Sens Environ, 194, 379-390, https://doi.org/10.1016/j.rse.2017.03.026, 2017.

Gardelle, J., Berthier, E., and Arnaud, Y.: Slight mass gain of Karakoram glaciers in the early twenty-first century, Nat Geosci, 5, 322-325, 10.1038/Ngeo1450, 2012.

Hanshaw, M. N. and Bookhagen, B.: Glacial areas, lake areas, and snow lines from 1975 to 2012: status of the Cordillera Vilcanota, including the Quelccaya Ice Cap, northern central Andes, Peru, The





Cryosphere, 8, 359-376, 10.5194/tc-8-359-2014, 2014.

Hugonnet, R., McNabb, R., Berthier, E., Menounos, B., Nuth, C., Girod, L., Farinotti, D., Huss, M., Dussaillant, I., Brun, F., and Kaab, A.: Accelerated global glacier mass loss in the early twenty-first century, Nature, 592, 726-731, 10.1038/s41586-021-03436-z, 2021.

Kääb, A., Treichler, D., Nuth, C., and Berthier, E.: Brief Communication: Contending estimates of 2003–2008 glacier mass balance over the Pamir – Karakoram – Himalaya, The Cryosphere, 9, 557-564, 10.5194/tc-9-557-2015, 2015.

Li, D., Shangguan, D., and Anjum, M. N.: Glacial Lake Inventory Derived from Landsat 8 OLI in 2016–2018 in China-Pakistan Economic Corridor, ISPRS International Journal of Geo-Information, 9, 10.3390/ijgi9050294, 2020.

Li, J. and Sheng, Y.: An automated scheme for glacial lake dynamics mapping using Landsat imagery and digital elevation models: a case study in the Himalayas, Int J Remote Sens, 33, 5194-5213, 10.1080/01431161.2012.657370, 2012.

Liu, Q., Mayer, C., Wang, X., Nie, Y., Wu, K., Wei, J., and Liu, S.: Interannual flow dynamics driven by frontal retreat of a lake-terminating glacier in the Chinese Central Himalaya, Earth Planet Sc Lett, 546, 10.1016/j.epsl.2020.116450, 2020.

Luo, W., Zhang, G., Chen, W., and Xu, F.: Response of glacial lakes to glacier and climate changes in the western Nyainqentanglha range, Sci Total Environ, 735, 139607, 10.1016/j.scitotenv.2020.139607, 2020.

Luo, Y. and Liu, Q.: Rapidly Changing Lake-Terminating Glaciers in High Mountain Asia: A Dataset from 1990 to 2022, Zenodo [dataset], https://doi.org/10.5281/zenodo.17369580, 2025.

Maurer, J. M., Schaefer, J. M., Rupper, S., and Corley, A.: Acceleration of ice loss across the Himalayas over the past 40 years, Science Advances, 5, eaav7266, doi:10.1126/sciadv.aav7266, 2019.

Mertes, J. R., Thompson, S. S., Booth, A. D., Gulley, J. D., and Benn, D. I.: A conceptual model of supraglacial lake formation on debris-covered glaciers based on GPR facies analysis, Earth Surface Processes and Landforms, 42, 903-914, https://doi.org/10.1002/esp.4068, 2017.

Quincey, D. J., Richardson, S. D., Luckman, A., Lucas, R. M., Reynolds, J. M., Hambrey, M. J., and Glasser, N. F.: Early recognition of glacial lake hazards in the Himalaya using remote sensing datasets, Global Planet Change, 56, 137-152, 10.1016/j.gloplacha.2006.07.013, 2007.



Salerno, F., Thakuri, S., D'Agata, C., Smiraglia, C., Manfredi, E. C., Viviano, G., and Tartari, G.: Glacial lake distribution in the Mount Everest region: Uncertainty of measurement and conditions of formation, Global Planet Change, 92-93, 30-39, 10.1016/j.gloplacha.2012.04.001, 2012.

Sato, Y., Fujita, K., Inoue, H., and Sakai, A.: Land- to lake-terminating transition triggers dynamic thinning of a Bhutanese glacier, The Cryosphere, 16, 2643-2654, 10.5194/tc-16-2643-2022, 2022.

Shugar, D. H., Burr, A., Haritashya, U. K., Kargel, J. S., Watson, C. S., Kennedy, M. C., Bevington, A. R., Betts, R. A., Harrison, S., and Strattman, K.: Rapid worldwide growth of glacial lakes since 1990, Nat Clim Change, 10, 939-945, 10.1038/s41558-020-0855-4, 2020.

Steiner, J., Armstrong, W., Kochtitzky, W., McNabb, R., Aguayo, R., Bolch, T., Maussion, F., Agarwal, V., Barr, I., Baurley, N. R., Cloutier, M., DeWater, K., Donachie, F., Drocourt, Y., Garg, S., Joshi, G., Guzman, B., Kutuzov, S., Loriaux, T., Mathias, C., Menounos, B., Miles, E., Osika, A., Potter, K., Racoviteanu, A., Rick, B., Sterner, M., Tallentire, G. D., Tielidze, L., White, R., Wu, K., and Zheng, W.: Global mapping of lake-terminating glaciers, Earth Syst. Sci. Data Discuss., 2025, 1-22, 10.5194/essd-2025-315, 2025.

Sugiyama, S., Skvarca, P., Naito, N., Enomoto, H., Tsutaki, S., Tone, K., Marinsek, S., and Aniya, M.: Ice speed of a calving glacier modulated by small fluctuations in basal water pressure, Nat Geosci, 4, 597-600, 10.1038/ngeo1218, 2011.

Sutherland, J. L., Carrivick, J. L., Gandy, N., Shulmeister, J., Quincey, D. J., and Cornford, S. L.: Proglacial Lakes Control Glacier Geometry and Behavior During Recession, Geophysical Research Letters, 47, 10.1029/2020gl088865, 2020.

Truffer, M. and Motyka, R. J.: Where glaciers meet water: Subaqueous melt and its relevance to glaciers in various settings, Reviews of Geophysics, 54, 220-239, 10.1002/2015rg000494, 2016.

Tsutaki, S., Sugiyama, S., Nishimura, D., and Funk, M.: Acceleration and flotation of a glacier terminus during formation of a proglacial lake in Rhonegletscher, Switzerland, Journal of Glaciology, 59, 559-570, 10.3189/2013JoG12J107, 2017.

Tsutaki, S., Fujita, K., Nuimura, T., Sakai, A., Sugiyama, S., Komori, J., and Tshering, P.: Contrasting thinning patterns between lake- and land-terminating glaciers in the Bhutanese Himalaya, The Cryosphere, 13, 2733-2750, 10.5194/tc-13-2733-2019, 2019.

Wang, X., Guo, X., Yang, C., Liu, Q., Wei, J., Zhang, Y., Liu, S., Zhang, Y., Jiang, Z., and Tang, Z.: Glacial lake inventory of high-mountain Asia in 1990 and 2018 derived from Landsat images, Earth





System Science Data, 12, 2169-2182, 10.5194/essd-12-2169-2020, 2020.

Worni, R., Huggel, C., and Stoffel, M.: Glacial lakes in the Indian Himalayas--from an area-wide glacial lake inventory to on-site and modeling based risk assessment of critical glacial lakes, Sci Total Environ, 468-469 Suppl, S71-84, 10.1016/j.scitotenv.2012.11.043, 2013.

Yao, T., Thompson, L., Yang, W., Yu, W., Gao, Y., Guo, X., Yang, X., Duan, K., Zhao, H., Xu, B., Pu, J., Lu, A., Xiang, Y., Kattel, D. B., and Joswiak, D.: Different glacier status with atmospheric circulations in Tibetan Plateau and surroundings, Nat Clim Change, 2, 663-667, 10.1038/nclimate1580, 2012.

Zhang, G., Yao, T., Xie, H., Wang, W., and Yang, W.: An inventory of glacial lakes in the Third Pole region and their changes in response to global warming, Global Planet Change, 131, 148-157, 10.1016/j.gloplacha.2015.05.013, 2015.

Zhang, G., Zheng, G., Gao, Y., Xiang, Y., Lei, Y., and Li, J.: Automated Water Classification in the Tibetan Plateau Using Chinese GF-1 WFV Data, Photogrammetric Engineering & Remote Sensing, 83, 509-519, 10.14358/pers.83.7.509, 2017.

Zhang, G., Bolch, T., Yao, T., Rounce, D. R., Chen, W., Veh, G., King, O., Allen, S. K., Wang, M., and Wang, W.: Underestimated mass loss from lake-terminating glaciers in the greater Himalaya, Nat Geosci, 16, 333-338, 10.1038/s41561-023-01150-1, 2023.

Zheng, G., Allen, S. K., Bao, A., Ballesteros-Cánovas, J. A., Huss, M., Zhang, G., Li, J., Yuan, Y., Jiang, L., Yu, T., Chen, W., and Stoffel, M.: Increasing risk of glacial lake outburst floods from future Third Pole deglaciation, Nat Clim Change, 11, 411-417, 10.1038/s41558-021-01028-3, 2021.